Precise 3d Modelling Using Combination Depth Maps Processing and Ground Control Point

Syetiawan, A.,[1] Maharani, M.,[2*] Nugroho, A. W.,[3] Setyo, R.,[3] Apriyanti, D.,[2] Agustian, M. P.[2] and Prihatin, S. M.[1]

[1]National Research and Innovation Agency, Jakarta-Bogor Km.46, Cibinong 16911, Indonesia
E-mail: agungsyetiawan@gmail.com, septinamarryanti.p@gmail.com
[2]Departement Geomatics Engineering, Universitas Pembangunan Nasional "Veteran", Padjajaran (SWK) 104 Road, Yogyakarta 55283, Indonesia
E- mail: monica.maharani@upnyk.ac.id,* dessy.apriyanti@upnyk.ac.id, putraagustian2108@gmail.com
[3]Ministry of Finance, Jakarta, Indonesia
E-mail: aditya.wahyu@kemenkeu.go.id, renaldi.setyo@kemenkeu.go.id
**Corresponding Author*

DOI: https://doi.org/10.52939/ijg.v21i4.4079

Abstract

The use of Unmanned Aerial Vehicles (UAV) has become increasingly popular compared to terrestrial mapping technologies such as terrestrial laser scanners (TLS) and Global Navigation Satellite Systems (GNSS), which are costly and have limited coverage. UAV offers quicker, wider coverage, and more detailed result. Typically, UAVs are used in precision agriculture, disaster mapping, and 3D building modeling. However, the accuracy of UAV 3D models often has issues. This study aims to improve the accuracy of 3D building facade models using a combination of depth maps and GCPs and to compare the results with direct measurements using a digital meter. The study was conducted at Kehati Building, Cibinong, Integrated Science Area Complex Area, BRIN. The study began with the acquisition of photo data using UAVs and the measurement of Ground Control Points (GCP). Subsequently, the aerial photos were processed into orthophotos with four processing scenarios based on the use of GCP and input mesh. Scenario 1 and 2 without using GCP, the difference is only in the input mesh. Scenario 1 uses dense cloud, while scenario 2 uses depth maps. On the other hand, scenarios 3 and 4 use GCP with the difference in the input mesh used. Finally, the geometric accuracy of the 3D building model produced from the four scenarios was tested. Accuracy tests showed that scenarios using GCP, as demonstrated in scenarios 3 and 4, had better RMSE which are 0.082 m and 0.064 m respectively. However, identification in scenario 3 was more difficult due to the imperfectly formed facade. Therefore, it can be concluded that the use of GCP significantly improves the dimensional accuracy of the facade.

Keywords: 3D Modeling, Dense Cloud, Depth Maps, Ground Control Point (GCP), Unmanned Aerial Vehicle (UAV)

1. Introduction

In the last few decades, the use of Unmanned Aerial Vehicle (UAV) technology has become more popular compared to terrestrial mapping technology. Terrestrial mapping such as terrestrial laser scanners (TLS) and positioning using the Global Navigation Satellite System (GNSS) are both still high-cost technologies with limited spatial coverage [1] and [2]. Even terrestrial technology such as GNSS only produces a very limited density of detail for objects above the earth's surface.

UAV offers speed, large scale area, and ease of data collection as well as detailed results when compared to terrestrial technology [3]. This is inseparable from the evolution of computer vision algorithms in image processing using photogrammetry. On the other hand, technological developments have made UAV equipment lighter, capable of carrying sensors in one vehicle. GNSS equipment is also installed on the UAV to obtain high accuracy map [4] and [5]. UAV is usually used for precise agriculture purposes [6] and [7], comprehensive mapping of disaster-affected areas [8] and [9], including the ease of constructing 3-dimensional buildings. The 3-dimensional building modelling can be used for the purposes of identifying building damage due to disasters [10], historical building management [11] and [12], and infrastructure monitoring [13] and [14].

UAV also can capture data using multiple angles of view. UAV surveys usually use nadir mode, aerial photography mode using a perpendicular angle (close to 90 degrees) to the object. However, the nadir method often cannot obtain detailed building areas. On the other hand, there is an oblique method of taking photos, namely using a tilted camera (generally 45°). The advantage of oblique mode is that building facades and other vertical objects can be seen well due to the tilt of the camera angle [15] and [16]. The combination of using nadir and oblique cameras can improve the depiction of the shape and surface of sub-vertical walls better [17]. Geometrically, the accuracy of 3D models of UAV is still often problematic. UAV point clouds without GCP produce absolute position accuracy of approximately 20 cm [18]. Other research also shows that building models from UAV produce an accuracy of around 18 cm for planimetric positions and 15 cm for height components [19]. It is necessary to improve strategies to obtain geometric accuracy of objects with high accuracy.

Generally, building a facade model can be done using a mesh from a point cloud or depth map. The problem is, in 3D modelling using UAV, many noisy point clouds are found, which affects the results of the facade mesh. In addition, an insufficient number of overlapping photos makes some point clouds have holes [20]. This greatly affects the quality of the building facade that is formed.

This research aims to produce a 3-dimensional building facade model using a combination of depth maps processing and the use of GCP. After that, the dimensions of the facade are measured from the results of the combination. The accuracy test of the 3-dimensional facade model was compared with direct measurements using a digital meter. The use of GCP is expected to increase the accuracy of facade dimensions. Apart from that, the use of depth maps is also expected to improve the appearance quality of the resulting building facade. In this study, aerial photo processing and acquisition are integrated. Include the use of GCP for orthorectification, multiple input mesh processing, and multiple angles of view with nadir and oblique modes. The main goal is to improve the facade's object accuracy and appearance.

2. Method

2.1 Research Area

The 3-dimensional building modelling research area was carried out in the Kehati Building, Cibinong Integrated Science Area Complex area, BRIN as can be seen in Figure 1. The Kehati Building is arranged into 3 buildings which are connected to each other in a relatively flat area. In this case, 3-dimensional modelling only uses one of the buildings on the north side where there are no trees or obstacles that could interfere with the data acquisition process. Therefore, 3-dimensional model data can be seen in its entirety when taking aerial photos.

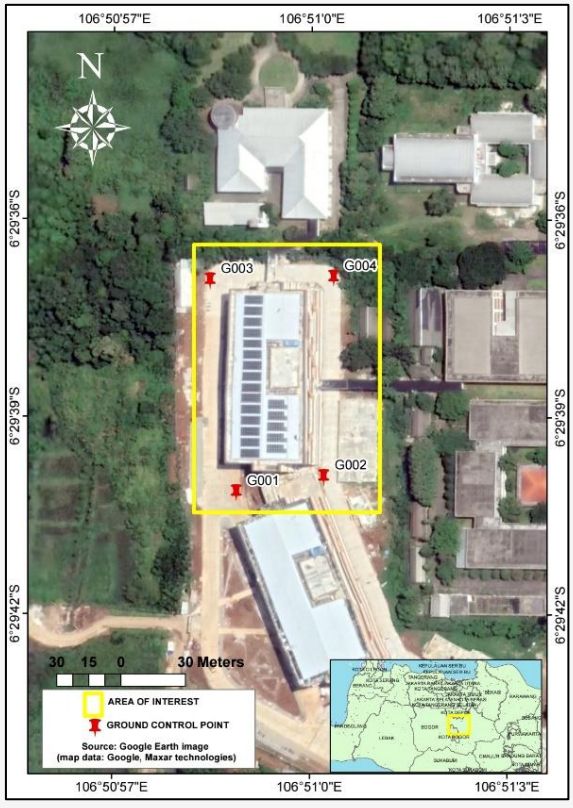

Figure 1: Location of Kehati-BRIN building

2.2 UAV Data Acquisition

Aerial photography was taken using an assembled multirotor type UAV DJI Phantom 4 Pro V2.0. The camera installed is a fixed lens CMOS camera with 20-megapixel resolution. Information related to the specifications of the UAV and the camera used can be seen in Table 1. The aerial photo acquisition process is carried out using two different camera orientations, namely nadir and oblique camera modes, as can be seen in Figure 2. The flight height used in this acquisition is 80m for nadir mode and 50m for camera oblique mode. The oblique mode flight altitude is lower compared to nadir mode to get a more detailed facade image. Taking aerial photos in nadir mode using the drone deploy application with overlap and side-overlap settings respectively, namely 80% and 70%, produces 250 images. The 3-dimensional mode parameter is also activated when setting the drone deploy. The aim is to obtain an oblique image from the perimeter of the flight mission plan, facing the centre of the building object.

Table 1: DJI Phantom 4 Pro V2.0 specification

Aircraft	
Take off Weight	1,375 g
Diagonal Size	350 mm
Max Service Ceiling Above Sea Level	19,685 ft (6,000 m)
Max Ascent Speed	6 m/s (S-mode); 5 m/s (P-mode)
Max Descent Speed	4 m/s (S-mode); 3 m/s (P-mode)
Max Pitch Angle	25° (P-mode); 35° (A-mode); 42° (S-mode)
Max Flight Time	Approx. 30 minutes
Operating Temperature Range	32° to 104° F (0° to 40℃)
Satellite Positioning Systems	GPS/GLONASS
Hover Accuracy Range	**Vertical:** ±0.1 m (with Vision Positioning) ±0.5 m (with GPS Positioning) **Horizontal:** ±0.3 m (with Vision Positioning) ±1.5 m (with GNSS positioning）
Battery Type	LiPo 4S (15.2 V)
Gimbal	
Stabilization	3-axis (pitch, roll, yaw)
Controllable Range	Pitch: -90° to +30°
Max Controllable Angular Speed	Pitch: 90°/s
Angular Vibration Range	±0.02°
Vision System	
Vision System	Forward/backward/downward
Velocity Range	≤31 mph (50 kph) at 6.6 ft (2 m) above ground
Altitude and Operating Range	0-33 ft (0-10 m)
Obstacle Sensory Range	2-98 ft (0.7-30 m)
Camera	
Sensor	1" CMOS; Effective pixels: 20 M; FOV 84°;
Lens	8.8 mm / 24 mm (35 mm format equivalent:24 mm); f/2.8 - f/11, auto focus at 1 m - ∞
ISO Range	Video:100-3200(Auto), 100-6400(Manual) Photo:100-3200(Auto), 100-12800(Manual)
Electronic Shutter Speed	8 - 1/8000 s
Operating Temperature Range	32° to 104° F （0° to 40℃）

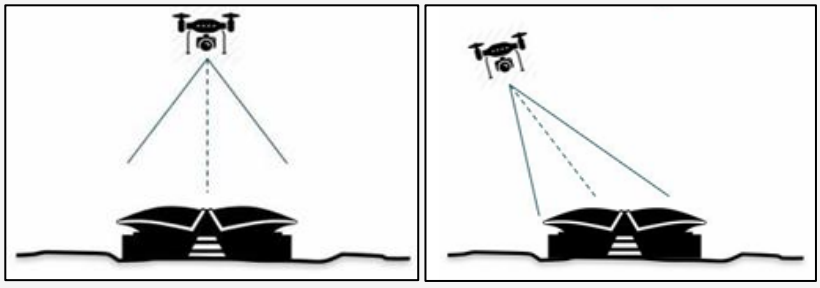

(a) (b)

Figure 2: UAV camera orientation: (a) nadir view, (b) oblique view

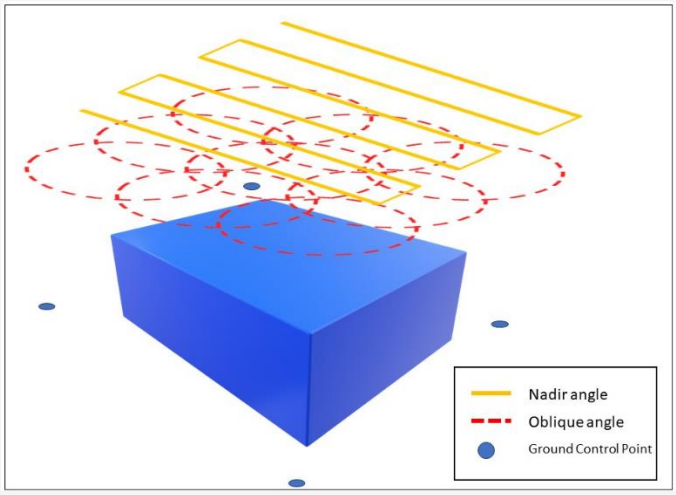

Figure 3: Aerial photo acquisition and ground control point in Kehati-BRIN building

Acquisition time takes about 12.5 minutes. The flight path is set in a South to North direction around the selected building with a total mapped area of around 5 hectares. Furthermore, another acquisition mode used is oblique mode, aimed at obtaining building facades that cannot be seen using nadir mode. On the other hand, oblique mode aerial photography was taken using the drone harmony application with the camera tilt angle set to 45°. The flight path is made to orbit around the mapped building with a distance between orbits of 50 m. There are 9 flight path orbits with an overlap setting of 60% to get a better 3-dimensional building model. The number of photos produced from oblique mode is 143 photos. An illustration of data acquisition using nadir and oblique modes in this research can be seen in Figure 3.

2.3 Measurement of Ground Control Points (GCP)

Ground control point (GCP) measurements were performed next, following the aerial photo acquisition procedure. Measurements of ground control points were made to create a three-dimensional model that had been georeferencing corrected. GCP points are distributed evenly across the building area with a total of 4 points. A geodetic type GNSS instrument, Leica Zeno GG04, was used to do GCP measurements. The GNSS measurement method uses a rapid static method with an observation interval of every 1s. The GCP data processing procedure connects to Continuously Operating Reference Stations (CORS) BAKO, utilizing a coordinate system that refers to the SRGI2013 datum, which is local horizontal and vertical datum applicable in Indonesia [21].

2.4 Aerial Photo Processing

Photogrammetry data was processed using the structure from motion (SfM) method in Agisoft Metashape (ver. 1.7.3). The obtained photos, which included both oblique and nadir images (143 and 250), were processed in a single project. There were 4 scenarios in aerial photo processing with differentiating parameters, namely dense cloud and depth maps input when creating the mesh and using GCP and without GCP during the georeferencing process. The scenarios in this research are shown in more detail in Table 2. In photogrammetric analyses, image processing often follows a simple workflow framework. Common tie points within the overlapping area are primarily used to perform bundle adjustments from the obtained images. The GCPs on the images perform the absolute orientation procedure after the sparse point cloud created by supplying the collinearity and coplanarity criteria with bundle adjustment [22]. In photogrammetry, absolute orientation is a basic technique that is crucial for transforming three-dimensional (3D) points from a local to a global (geodetic) coordinate reference system [23]. Next, interior orientation parameters were estimated using self-calibrating in Agisoft for all processing scenarios. In the 'Align Photos' process, the parameters used to create sparse clouds are as follows: accuracy = high, key point limit = 60,000, and check the Adaptive camera model fitting section. The next stage is to carry out GCP pricking for scenarios 3 and 4. A dense cloud is then built using high accuracy parameters and mild filtering depth to get denser point cloud. In addition to producing dense clouds, the dense cloud build process also produces depth maps.

Table 2: Combination of 3D building modelling processing

No	Type	Georeferencing		Input mesh	
		GCP	No-GCP	Dense cloud	Depth maps
1.	Scenario 1	-	✓	✓	-
2.	Scenario 2	-	✓	-	✓
3.	Scenario 3	✓	-	✓	-
4.	Scenario 4	✓	-	-	✓

Depth maps are generated from Multi-View Stereo from overlapping sequential photos [24] and [25]. Depth maps are very useful for producing accurate 3d reconstruction [26]. After the point cloud and depth maps are produced, building facade was constructed. To achieve better 3D result, the building facade was constructed using high quality parameters mesh and arbitrarily chosen surface type. For scenarios 1 and 3 the mesh was built using dense cloud, while for scenarios 2 and 4 using depth maps.

2.5 Validation of 3-Dimensional Building Geometry

The aerial photos, both nadir and oblique, are then processed to produce a building facade in mesh format. Next, the dimensions of the building were then measured using the ContextCapture viewer software. The process of validating the 3-dimensional building geometry resulting from UAV acquisition is carried out by comparing the 3-dimensional building results with direct measurements in the field. Calculation of 3D modeling accuracy uses the root mean square error (RMSE) equation, as can be seen in Equation 1.

$$RMSE = \sqrt{\frac{\sum (S_i - S_m)^2}{n}}$$

Equation 1

Where S_i is the dimension of the object using a laser distance meter, S_m is the dimension of the object resulting from the UAV, and S is the number of validation samples. Validated building geometry includes wall width, windows, floor width, height, facade decoration on all sides of the building. In this case, direct measurement of building dimensions uses a SNDWAY Green Laser-50m digital laser meter and a 50m long iron plate measuring tape. The total geometry validation sample amounted to 67 building geometry measurements, as can be seen in Figure 4.

3. Result and Discussion

3.1 GCP Processing Result

Less than 400 meters separated the base station from the GCPs, and baseline measurements were made for sessions longer than 20 minutes. The computation of the baselines produced fixed phase ambiguity solutions for all points, with horizontal precision ranging from 5-12 mm and vertical precision ranging from 1-19 mm. Meanwhile, RMSE GNSS processing produces accuracy ranging from 8-16 mm. These results are good enough to obtain a thorough 3D model of the building (Table 3).

3.2 Aerial Photo Result

The combination of nadir and oblique measurements produces tie points with a total of 216,063 points for full area, as can be seen in Figure 5(a). Unfortunately, high number of close images induces strong noise and affected on accuracy 3D modelling [27]. So, it would be better to remove outlier tie points manually. The number of points is the result of the data filtering process for non-building areas and several outliers points a total of 67,984 points (Figure 5(b)). Once the tie point noise has been reduced, a more accurate mesh will be produced.

3.3 3D Modelling Result

The results of forming a 3D building model using a mesh model from dense cloud and depth maps can be seen in Figure 6. The total faces formed for the mesh model from depth maps were 2,210,411 with 13 similar vertices. Meanwhile, for the mesh model using dense cloud the total faces were 2,114,712 with similar vertices 11. Making 3D models based on Depth Maps produces better small details of the facade compared to dense cloud results. In the dense cloud results, the facade wall surface still appears to contain artifacts. Even the facade looks incomplete, like it has holes in several parts. The results of the 3D building model accuracy test using laser distance meter measurements are presented in Table 4. Only 47 samples out of a total of 67 digital meter measurement samples can be used to test the accuracy of the 3D model. There were 20 samples that could not be identified in the 3D model because the 3D model did not perfectly form the building facade. Scenario 1 produces an RMSE value of 0.135 m with an R square value of 99.97%. The largest residual is 0.08 in sample 11 in the facade dimension with a distance of ~8 m. Furthermore, Scenario 2 produces an RMSE value of 0.087 m with an R square value of 99.97%.

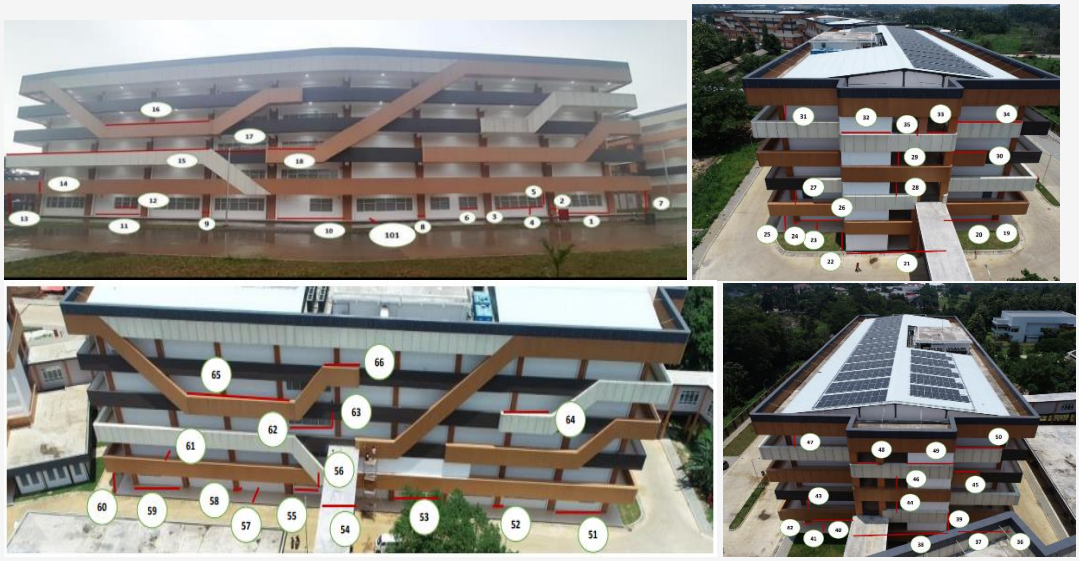

Figure 4: Taking field validation points

Table 3: GCP processing result

ID	Easting (m)	Northing (m)	Heigh (m)	Ambiguity solution	Hor. Precision (m)	Vert. Precision (m)	RMSE (m)
G001	704,545.849	9,281,759.464	158.102	Fixed	0.005	0.001	0.008
G002	704,586.472	9,281,766.620	158.125	Fixed	0.012	0.019	0.016
G003	704,533.631	9,281,858.322	158.152	Fixed	0.008	0.014	0.010
G004	704,591.043	9,281,859.576	158.100	Fixed	0.007	0.010	0.010

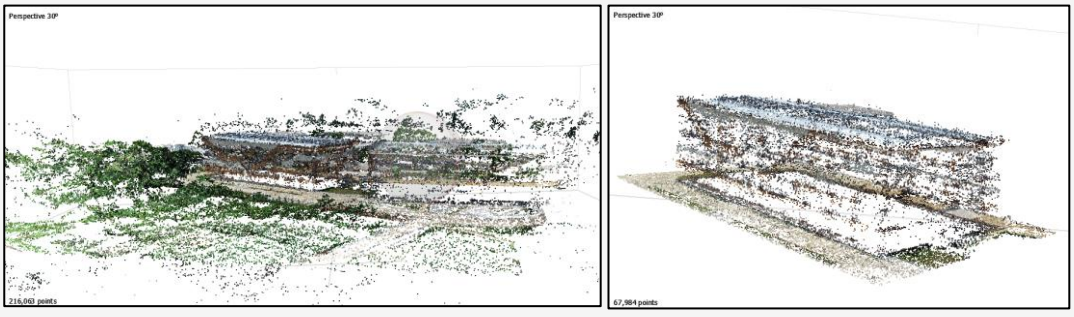

(a) (b)

Figure 5: Tie point results from nadir and oblique views: (a) full points (b) filtering points

Table 4: Accuracy testing of 3D models with various scenarios

Type	Min (m)	Max (m)	Mean (m)	RMSE (m)
Scenario 1	0.001	0.081	0.018	0.135
Scenario 2	0.001	0.049	0.007	0.087
Scenario 3	0.001	0.070	0.007	0.082
Scenario 4	0.001	0.049	0.004	0.064

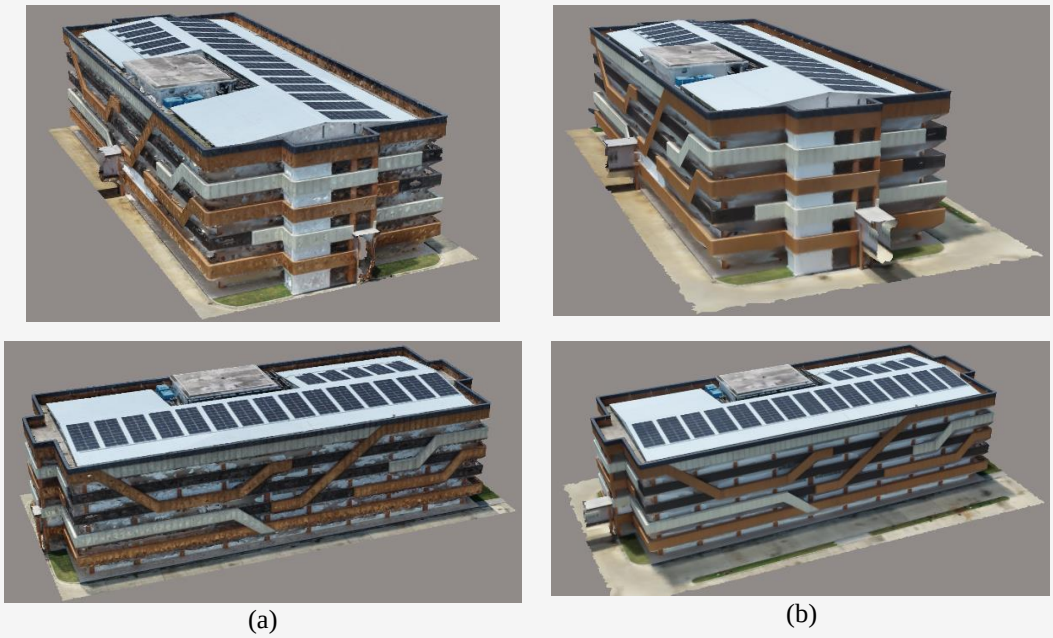

(a) (b)

Figure 6: 3D mesh model (a) dense cloud (b) depth maps

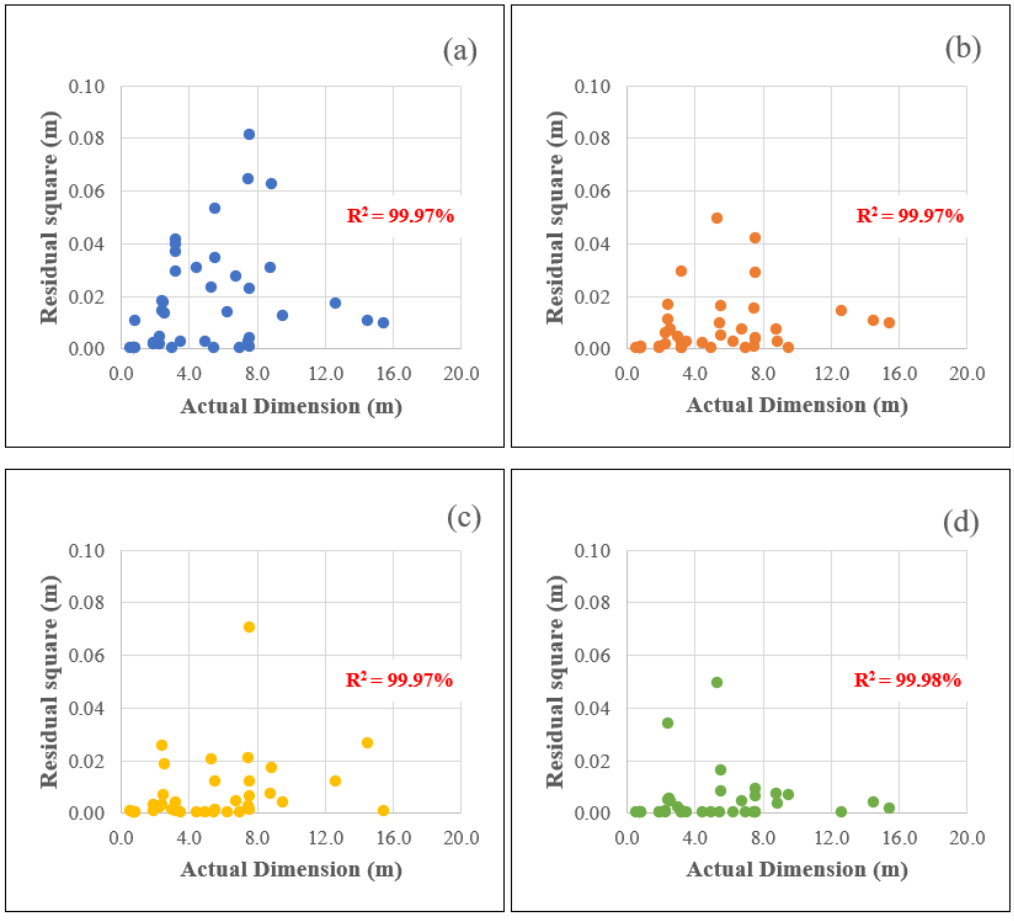

Figure 7: Correlation between actual dimension and residual squared:
(a) scenario 1 (b) scenario 2 (c) scenario 3 (d) scenario 4


Front facade

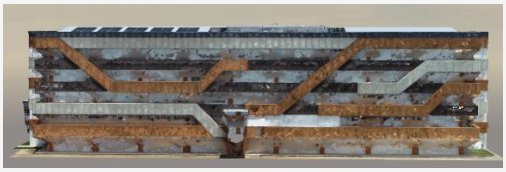
Front facade


Side facade

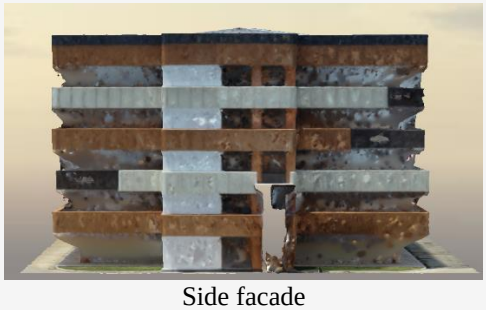
Side facade

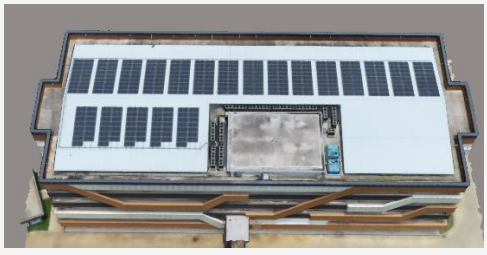
Top of building

(a)

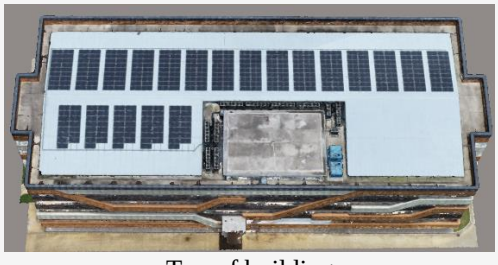
Top of building

(b)

Figure 8: Façade visualization derived from UAV 3D modeling: (a) depth maps (b) dense Cloud

Table 5: Visual facade from dense cloud and depth maps result

Source	Visual Appearance					
	Semantics				Texture	
	Window	Door	Pillar	Roof and Wall Facade	Shape	Color
Dense Cloud	10 are partially formed and 22 are not formed	11 doors are not perfectly formed	20 building pillars are formed	The roof and wall facade are formed	Surface with large hole	Realistic
Depth map	10 are partially formed and 22 are not formed	11 doors are not perfectly formed	20 building pillars are formed	The roof and wall facade are formed	Smooth	Realistic

The largest residual is 0.05 in sample 30 in the facade dimension with a distance of ~5 m. Then, Scenario 3 produces an RMSE value of 0.082 m with an R square value of 99.97%. The largest residual is 0.07 in sample 11, the same as in scenario 1, namely the facade with a distance of ~8 m. Finally, Scenario 4 produces an RMSE value of 0.064 m with an R square value of 99.98%. The largest residual is 0.05 in sample 30 in the facade dimension with a distance of ~5 m. Based on Figure 7, scenario 1 produces a residual square with an imprecise distribution. This is because the mesh model from Dense Cloud produces a facade with a rough plane pattern. The facade plane looks like it is uneven, due to the imperfection of the tie points formed. The use of GCP in scenarios 3 and 4 produces better RMSE accuracy compared to without GCP (scenarios 1 and 2).

Using a similarity transformation consisting of one scaling parameter, three rotation angles, and three translation vector parameters, GCP shows the geometric relationships between 3D points in the local and global coordinate reference systems [28]. These seven parameters are used to adjust real-world objects. However, in order to accurately generate 3D surface reconstruction, GCP can remove distortion caused by the dome effect [29].

Even though in scenario 3 the RMSE is better, the identification process is more difficult because the facade formed is not perfect. In terms of the visual semantic appearance of facade ornaments such as doors, windows, pillars, roofs, and wall facades, the results of both processing using dense clouds and depth maps produce almost the same visualization results. A summary of facade ornaments can be seen in Table 5. In terms of texture, the results of depth maps are better because they produce a 3D surface model with minimal perforated areas and have a smoother texture compared to dense clouds. A more complete visual comparison of the results of facade ornaments between dense clouds and depth maps can be seen in Figure 8. Facade areas that are not photographed during UAV acquisition will produce perforated areas due to the unavailability of point clouds. High-density point clouds are needed to produce 3D models of complex building facades [30] and [31]. This high density can be obtained from UAV multilooking capture.

4. Conclusions

The computation of the GCP produced fixed phase ambiguity solutions for all points, with capable horizontal and vertical accuracy. These GCP points can be used for the georeferenced process on aerial photos. On the other hand, to produce a realistic mesh, it is necessary to carry out a tie point noise filtering process. The combination of GCP and mesh input using Depth Maps (Scenario 4) produces the best RMSE compared to other scenarios, namely 0.064 m. In this case, the use of Depth Maps produces better RMSE accuracy compared to Dense Cloud because the facade plane is well formed, making it easy to identify facades. The use of GCP has been proven to increase the dimensional accuracy of the facade (as can be seen in scenarios 3 and 4). This is because GCP arranges all the tie points formed in the most accurate position possible, thereby producing a precise 3D model.

It has been demonstrated that integrating UAV data collection and processing improves the 3D object accuracy and appearance of facades. Building information modeling (BIM), building taxes, and applications that need precise facade information all depend greatly on knowledge of 3D object accuracy.

Acknowledgment

This research is an implementation of collaboration between UPN "Veteran" Yogyakarta and the National Research and Innovation Agency of Indonesia (BRIN) through the MBKM (Merdeka Belajar Kampus Merdeka) program. In addition, the authors would also like to thank the Geospatial Information Agency for providing UAV data.

References

[1] Barba, S., Barbarella, M., Di Benedetto, A., Fiani, M. and Limongiello, M., (2019). Comparison of UAVS Performance for a Roman Amphitheatre Survey: The Case of Avella (Italy). *The International Archives of the Photogrammetry, Remote Sensing and Spatial Information Sciences*, *Vol. XLII-2/W11*, 179–186. https://doi.org/10.5194/isprs-archives-XLII-2-W11-179-2019.

[2] Khanal, M., Hasan, M., Sterbentz, N., Johnson, R. and Weatherly, J., (2020). Accuracy Comparison of Aerial Lidar, Mobile-Terrestrial Lidar, and UAV Photogrammetric Capture Data Elevations over Different Terrain Types. *Infrastructures*, Vol. 5(8). https://doi.org/10.3390/infrastructures5080065.

[3] Park, J. K. and Lee, K. W., (2022). Geospatial Information Construction and Usability Evaluation Using Nadir Image and Oblique Image. *Sensors and Materials*, Vol. 34(7). https://doi.org/10.18494/SAM3728.

[4] Thanh, P., Elshewy, M., Long, N., and Thom, T. (2023). Creation and Assessment of a Topographic Map from Unmanned Aerial Vehicle Data in Thanh Son District, Vietnam. *International Journal of Geoinformatics*, Vol. 19(3), 57–66. https://doi.org/10.52939/ijg.v19i3.2605.

[5] Luong, N., Tran, D., and Doung, C. (2023). Applying GIS and Geospatial Measurement Technologies in Construction Data Management in Vietnam: A Case Study of Hanoi University of Civil Engineering's Campus. *International Journal of Geoinformatics*, Vol. 19(10), 40–50. https://doi.org/10. 52939/ijg.v19i9.2879.

[6] Syetiawan, A. and Haidar, M., (2019). Pemetaan Perkebunan Sawit Rakyat dari Foto Udara Nonmetrik Menggunakan Analisis Berbasis Objek (Mapping of Smallholder Oil Palm Plantations from Nonmetric Aerial Photos Using Object-Based Analysis). *Majalah Ilmiah Globë*, Vol. 21(1), 53–62. https://doi.org/10.24895/MIG.2019.21-1.990.

[7] Tsouros, D. C., Bibi, S. and Sarigiannidis, P. G., (2019). A Review on UAV-Based Applications for Precision Agriculture. *Information*, Vol. 10(11). https://doi.org/10.3390/info10110349.

[8] Niethammer, U., James, M. R., Rothmund, S., Travelletti, J. and Joswig, M., (2012). UAV-based Remote Sensing of the Super-Sauze Landslide: Evaluation and Results. *Engineering Geology*, Vol. 128, 2-11. https://doi.org/10.1016/j.enggeo.2011.03.012.

[9] Mohd Daud, S. M. S., Mohd Yusof, M. Y. P., Heo, C. C., Khoo, L. S., Chainchel Singh, M. K., Mahmood, M. S. and Nawawi, H., (2022). Applications of Drone in Disaster Management: A Scoping Review. *Science and Justice*, Vol. 62(1), 30-42. https://doi.org/10.1016/j.scijus.2021.11.002.

[10] Nagasawa, R., Mas, E., Moya, L. and Koshimura, S., (2021). Model-based Analysis of Multi-UAV Path Planning for Surveying Postdisaster Building Damage. *Scientific Reports*, Vol. 11(1). https://doi.org/10.1038/s41598-021-97804-4.

[11] Chetverikov, B., Trevoho, I., Prokhorchuk, O., Vladimirov, S., and Herasymchuk, P. (2024). Synergy of UAV Aerial Survey Methods and LiDAR Scanning for the Study of Planar Objects of Historical and Cultural Heritage. *International Journal of Geoinformatics*, Vol. 20(9), 98–111. https://doi.org/10.52939/ijg.v20i9.3551.

[12] Karachaliou, E., Georgiou, E., Psaltis, D. and Stylianidis, E., (2019). UAV for Mapping Historic Buildings: From 3d Modelling to BIM. *The International Archives of the Photogrammetry, Remote Sensing and Spatial Information Sciences*, Vol. *XLII-2/W9*, 397-402. https://doi.org/10.5194/isprs-archives-XLII-2-W9-397-2019.

[13] Máthé, K. and Buşoniu, L., (2015). Vision and Control for UAVs: A Survey of General Methods and of Inexpensive Platforms for Infrastructure Inspection. *Sensors*, Vol. 15(7), 14887–14916. https://doi.org/10.3390/s150714887.

[14] Morgenthal, G., Hallermann, N., Kersten, J., Taraben, J., Debus, P., Helmrich, M. and Rodehorst, V., (2019). Framework for Automated UAS-based Structural Condition Assessment of Bridges. *Automation in Construction*, Vol. 97, 77–95. https://doi.org/https://doi.org/10.1016/j.autcon.2018.10.006.

[15] Gerke, M., (2009). Dense Matching in High Resolution Oblique Airborne Images. *The International Archives of the Photogrammetry, Remote Sensing and Spatial Information Sciences*, Vol. 38, 77–82. https://www.isprs.org/proceedings/xxxviii/3-w4/pub/cmrt09_77.pdf.0.

[16] Bannakulpiphat, T., and Santitamnont, P. (2024). A Comparative Analysis of Camera Rig Parameters in Photogrammetric Software for Small-Format Oblique Camera System on Unmanned Aerial Vehicle. *International Journal of Geoinformatics*, Vol. 20(2), 1–10. https://doi.org/10.52939/ijg.v20i2.3059.

[17] Rossi, P., Mancini, F., Dubbini, M., Mazzone, F., and Capra, A. (2017). Combining nadir and oblique UAV imagery to reconstruct quarry topography: methodology and feasibility analysis. *European Journal of Remote Sensing*, Vol. 50(1), 211–221. https://doi.org/10.1080/22797254.2017.1313097.

[18] Neitzel, F. and Klonowski, J., (2011). Mobile 3d Mapping with a Low-Cost UAV System. *The International Archives of the Photogrammetry, Remote Sensing and Spatial Information Sciences*, Vol. *XXXVIII-1*, 39-44. https://doi.org/10.5194/isprsarchives-XXXVIII-1-C22-39-2011.

[19] Jarzabek-Rychard, M. and Karpina, M., (2016). Quality Analysis on 3d Buidling Models Reconstructed from UAV Imagery. *The International Archives of the Photogrammetry, Remote Sensing and Spatial Information Sciences*, Vol. *XLI-B1*, 1121–1126. https://doi.org/10.5194/isprs-archives-XLI-B1-1121-2016.

[20] Verykokou, S., Doulamis, A., Athanasiou, G., Ioannidis, C. and Amditis, A., (2016). UAV-based 3D Modelling of Disaster Scenes for Urban Search and Rescue. *2016 IEEE International Conference on Imaging Systems and Techniques (IST)*, 106–111. https://doi.org/10.1109/IST.2016.7738206.

[21] Syetiawan, A., Ramdani, D., Safii, A. N., Ardhitasari, Y., Gaol, L. and Annuriah, I., (2019). Development of Parameter Transformation of Indonesian Geospatial Reference System 2013. *KnE Engineering*, Vol. *4*(3 SE-Articles). https://doi.org/10.18502/keg.v4i3.5828.

[22] Kraus, K., (2007). *Geometry from Images and Laser Scans*. Berlin, Boston: De Gruyter, 2007. https://doi.org/10.1515/9783110892871.

[23] Yan, L., Wan, J., Sun, Y., Fan, S., Yan, Y. and Chen, R., (2016). A Novel Absolute Orientation Method Using Local Similarities Representation. *ISPRS International Journal of Geo-Information*, Vol. 5(8). https://doi.org/10.3390/ijgi5080135.

[24] Campbell, N. D. F., Vogiatzis, G., Hernández, C. and Cipolla, R., (2008). Using Multiple Hypotheses to Improve Depth-Maps for Multi-View Stereo BT - Computer Vision – ECCV 2008. In D. Forsyth, P. Torr, and A. Zisserman (Eds.), *Lecture Notes in Computer Science* (pp. 766–779). Springer Berlin Heidelberg.

[25] Fuhrmann, S. and Goesele, M., (2011). Fusion of Depth Maps with Multiple Scales. *ACM Transactions on Graphics*, Vol. 30(6), 1-8. https://doi.org/10.1145/2070781.2024182.

[26] Liu, Y., Cao, X., Dai, Q. and Xu, W., (2009). Continuous Depth Estimation for Multi-View Stereo. *2009 IEEE Conference on Computer Vision and Pattern Recognition*, 2121–2128. https://doi.org/10.1109/CVPR.2009.5206712.

[27] Barba, S., Barbarella, M., Di Benedetto, A., Fiani, M., Gujski, L. and Limongiello, M., (2019). Accuracy Assessment of 3D Photogrammetric Models from an Unmanned Aerial Vehicle. *Drones*, Vol. 3(4). https://doi.org/10.3390/drones3040079.

[28] Mikhail, E. M., Bethel, J. and McGlone, J. C., (2001). *Introduction to Modern Photogrammetry*. Wiley.

[29] Oniga, V. E., Pfeifer, N. and Loghin, A. M., (2018). 3D Calibration Test-Field for Digital Cameras Mounted on Unmanned Aerial Systems (UAS). *Remote Sensing*, Vol. 10(12). https://doi.org/10.3390/rs10122017.

[30] Alidoost, F. and Arefi, H., (2015). An Image-Based Technique for 3d Building Reconstruction Using Multi-View UAV Images. *The International Archives of the Photogrammetry, Remote Sensing and Spatial Information Sciences*, Vol. *XL-1/W5*, 43–46. https://doi.org/10.5194/isprsarchives-XL-1-W5-43-2015.

[31] Malihi, S., Valadan Zoej, M. J. and Hahn, M., (2018). Large-Scale Accurate Reconstruction of Buildings Employing Point Clouds Generated from UAV Imagery. *Remote Sensing*, Vol. 10(7). https://doi.org/10.3390/rs10071148.